# Polyethylene Duct Cracking on Posttensioning Tendons in Florida Segmented Bridges

Jorge Suarez[1]; Jingyu Zhang[2]; Grace Hsuan[3]; and William Hartt[4]

**Abstract:** During the past 20-plus years, designs based on the post-tension segmental concrete box concept have evolved to become prominent in bridge construction. Critical to the safety and longevity of such structures is the integrity of post-tensioning tendons. However, during the past five years, several Florida bridges have suffered tendon deterioration and failure because of strand corrosion at grout voids in which bleed water had accumulated. In some cases, the high-density polyethylene (HDPE) ducts within which the grouted strands reside had cracked. Although none of the tendon failures to date have been related to the HDPE duct cracking, left unaddressed moisture, chlorides, and oxygen will invariably corrode strands in the long-term. In order to assess the cause(s) and mechanism(s) of HDPE duct cracking, fatigue tests were performed upon duct samples retrieved from representative bridges and the results were compared with those from (1) material property determinations of the corresponding ducts, (2) experiments on simulated tendons that were subjected to thermal cycling, and (3) finite element analyses. Based on the outcomes, a mechanism is proposed for the duct cracking and time-to-cracking projections are made for ducts that are still sound.

**DOI:** 10.1061/(ASCE)0899-1561(2006)18:4(581)

**CE Database subject headings:** Polyethylene; Cracking; Florida; Bridges; Tension.



## Background

During the past several decades, segmental construction using precast concrete elements has become a preferred design and construction method for bridges. Segments used in bridge construction are precast, placed in position according to the design of the sub- or superstructure, and held together by posttensioned cables that are either internal (contained within embedded ducts) or external to the concrete but within the segment interior. These tendons consist of (1) multiple seven-wire high-strength steel cables that conform to ASTM A416 (typically with a 11,860 MPa [270 ksi] minimum ultimate strength); (2) a high-density polyethylene (HDPE) duct within which the cables are strung; and (3) a cementitious grout fill within the duct. For a superstructure, individual cables terminate at a relatively high position within bulkheads at the end of a precast section and traverse and hold together six or more sections by passing through periodically spaced deviation blocks along the base. In segmental bridge construction tendon integrity is critical to the safe operation and structural integrity of the bridge.

In the summer of 1999, a failed tendon was disclosed within the Niles Channel Bridge in the Florida Keys. Analysis revealed severe corrosion near one of the anchorage termination blocks. Tendon corrosion was also found on other cables within this bridge. Similar severe tendon corrosion and failed tendons were subsequently found on the Sunshine Skyway and Mid-Bay bridges located in the Tampa and Florida panhandle regions, respectively.

Most instances of strand corrosion were attributed to accumulation of bleed water at locations of grout subsidence and within air voids (Ghorbanpoor and Madathanapalli 1993; Tabatabai et al. 2000). However, cracking in the HDPE ducts may also contribute to the strand corrosion. Factors that could lead to cracking of HDPE ducts include (1) inferior resin properties; (2) inadequate response of the duct to environmental factors (temperature variations in particular); and (3) the manner with which the duct interacts with the grout. Numerous longitudinal splits were apparent on the ducts of the Mid-Bay Bridge (Corven 2001). Similar phenomena have also occurred on ducts in the Skyway Bridge but rarely in the Niles Channel and other Keys bridges. Although the ducts, unlike the strands, are not poststressed, and as such have no load-bearing function, still such splitting is likely to render strands more exposed to the environment and resultant corrosion may compromise the long-term integrity of the bridge. Preliminary analyses have indicated that the relatively poor performance of the Mid-Bay Bridge ducts resulted from (1) an inferior duct resin; and (2) stresses arising from thermal expansion/contraction combined with compounding effects associated with grout voids (Hartt and Venugopalan 2002). A comprehensive evaluation of the duct-cracking problem and future direction recommendations for segmental bridge construction have been made (Corven 2002).

The present paper reports the results of experiments and analyses that were performed to understand the mechanism of duct

[1]Graduate Student, Center for Marine Materials, Florida Atlantic Univ., Sea Tech Campus, 101 North Beach Road, Dania Beach, FL 33004.

[2]Graduate Student, Civil, Architectural, and Environmental Engineering, Drexel Univ., 3141 Chestnut Street, Philadelphia, PA 19104.

[3]Associate Professor, Civil, Architectural, and Environmental Engineering, Drexel Univ., 3141 Chestnut Street, Philadelphia, PA 19104.

[4]Professor and Director, Center for Marine Materials, Florida Atlantic Univ., Sea Tech Campus, 101 North Beach Road, Dania Beach, FL 33004.

Note. Associate Editor: Kiang-Hwee Tan. Discussion open until January 1, 2007. Separate discussions must be submitted for individual papers. To extend the closing date by one month, a written request must be filed with the ASCE Managing Editor. The manuscript for this paper was submitted for review and possible publication on January 26, 2005; approved on June 28, 2005. This paper is part of the ***Journal of Materials in Civil Engineering***, Vol. 18, No. 4, August 1, 2006. ©ASCE, ISSN 0899-1561/2006/4-581–587/$25.00.

**Table 1.** Acquired Field Samples

| Bridge | County | Age, years |
|---|---|---|
| Mid Bay (MB) | Okaloosa | 10 |
| Skyway (SSK) | Pinellas | 17 |
| Seven Mile (SM) | Monroe | 21 |
| Long Key (LK) | Monroe | 22 |
| 3408-1 | — | New |
| 3408-2 | — | New |

cracking and where it has occurred and to project future performance of ducts that are still sound.

## Experimental Procedure

### Materials

Duct samples were acquired from four bridges, as listed in Table 1. These were supplemented by new, black, smooth HDPE (PE3408 resin) (Pressure Pipe Institute 2005) samples, designated 3408-1 and 3408-2, from two different sources. Material properties of the ducts were assessed according to either the applicable bridge specification or AASHTO specification and the associated ASTM one, as listed in Table 2.

### Fatigue Testing

Specimen preparation involved retrieving duct samples from the six sources listed in Table 1 and cutting these into small pieces that were then compression molded into 6.4 mm thick plaque. The molding was completed according to ASTM D4703 at a cooling rate of 15±2°C. Specimens 102 mm long by 25 mm wide were cut from the plaque using a die. A 1.3 mm deep notch was introduced at the center of the specimens at a notching rate of 0.5 mm/min.

Fatigue tests were performed by three-point bending using an Instron Model 1331 machine under load control at 3 Hz, an initial load of 44 N, and a half-sine wave loading function. Failure was defined as the number of cycles corresponding to a vertical specimen deflection of 25 mm. Maximum loads of 88–490 N (load range 44–441 N) were employed, and the corresponding stress ($\sigma$) was calculated using the equation

$$\sigma = \frac{3PL}{2bd^2} \quad (1)$$

where $P$=applied load; $L$=span length (51 mm); $b$=specimen cross section; and $d$=specimen thickness.

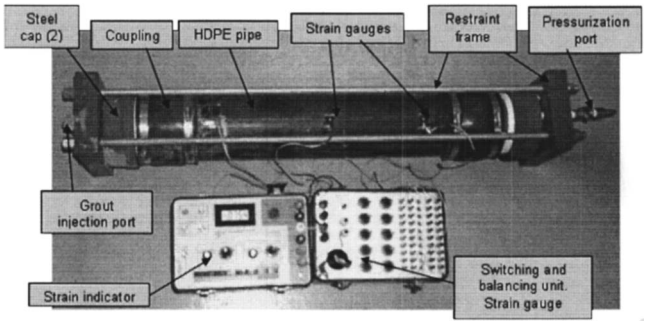


**Fig. 1.** Instrumented simulation tendon duct specimen

### Experiments to Simulate Thermal Response of Tendons

Two 0.55 m long simulated tendons were prepared using sections of PE3408 pipes (same material as 3408-1 in Table 1) with a nominal diameter of 102 mm (4.0 in.). The SDR (diameter-to-wall thickness ratio) of the pipes was 21 and 17 for Specimen B2 and Specimen B4, respectively. The diameter of the strands was 12.7 mm (0.5 in.). Strain gauges and thermocouples were mounted at various locations on the assembled tendon. Fig. 1 shows an assembled tendon, including a restraining frame, and Fig. 2 illustrates the locations of strain gauges and thermocouples. Fabrication and experiments involved the following steps:

1. Grout injection under pressure such that a void channel resulted along the upper duct interior;
2. Grout setting under pressure;
3. Pressure release; and
4. Cyclic exposure to different temperatures.

Both specimens were grouted at 0.414 MPa (60 psi), and the pressure was maintained for approximately 22 h. The specimens were then subjected to a 14-day thermal cycle, which consisted of seven days in a freezer at −39°±2°C followed by seven days outdoors (temperature between 20 and 35°C at the time of measurement). Recognizing that for a ventilated, sheltered outdoor Florida exposure, the maximum range of temperature change varies from about 36°C (2 to 38°C) in the keys to 50°C (−9 to 41°C) in the northern region. Thus, the changes of temperature in the field are less than that in the laboratory-simulated tendon exposures, in which the range was from 59 to 74°C depending upon the outdoor temperature. However, it can be reasoned that since the simulated tendons were prepared and pressurized indoors (22–24°C), duct strain gauge outputs that occurred during exposure at higher temperatures reflected thermal expansion of the duct only and not mechanical strains because the coefficient of thermal expansion of the duct exceeded that of the grout. On this basis, mechanical strains introduced in the duct occurred only in conjunction with thermal cycling from −39 to 22–24°C such that

**Table 2.** Applicable Specifications for the Field Duct Samples

| Bridge | Source | Material specification |
|---|---|---|
| MB | Construction specification | ASTM D3350 with a cell classification PE 345433C. |
| SSK | No material specification available | AASHTO specification was used. |
| | | ASTM D3350 with a cell classification PE 345433C. |
| SM | Supplied by duct manufacturer | ASTM D3350 with a cell classification PE 335433C. |
| LK | Printed on the exterior wall | PE 3406 and PE 3408 |



J. Mater. Civ. Eng., 2006, 18(4): 581-587

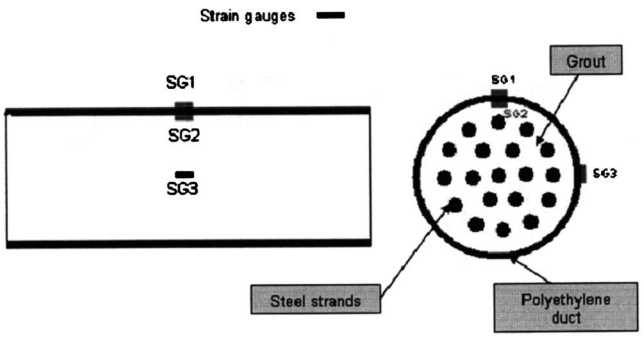


**Fig. 2.** Tendon segment specimens with location of strain gauges

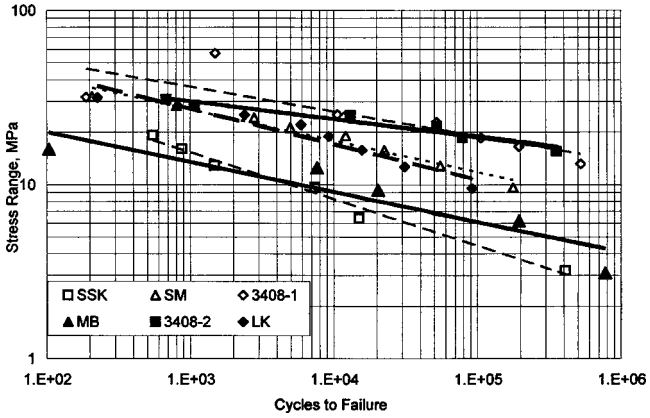


**Fig. 3.** Fatigue data for various duct samples

the range was 61–63 °C, which is about 20–70% greater than what should occur in service (see above).

## Results and Discussion

### Material Properties

Table 3 summarizes the results of the material property determinations. The HDB (hydrostatic design basis) test and SCGR (slow crack growth resistance) test were not performed; however, the single point notched constant tensile load (SP-NCTL) and oxidative induction time (OIT) tests were added. A detailed description of the tests and test results are reported elsewhere (Hartt et al. 2005). It is apparent that the failure times of the SP-NCTL tests for duct samples from MB and SSK are relatively poor in comparison to those from SM and LK and that those for the two new PE3408 ducts are the best.

### Fatigue Tests

Results of the fatigue tests are presented as a plot of stress range versus cycles to failure (S-N plot) in Fig. 3. These conform to a power law relationship according to the expression

$$\Delta\sigma = AN^b \tag{2}$$

where $\Delta\sigma$=stress range; $N$=cycles to failure; and $A$ and $b$=material constants. The MB and SSK specimens exhibited

**Table 3.** Material Properties of Field Duct Samples from the Four Bridges

| | | MB and SSK | | | | SM | | | LK | | | |
|---|---|---|---|---|---|---|---|---|---|---|---|---|
| | | | | MB | SSK | | | | Cell class | | Measurement | |
| Property | Test method | Cell class | Requirement | Measurement | | Cell class | Requirement | Measurement[d] | PE3408/3406 | Requirement | PE3408 | PE3406 |
| Density, g/cc | ASTM D792 | 3 | >0.940–0.955 | P | | 3 | >0.940–0.955 | P | 3 | >0.940–0.955 | P | |
| Melt index, g/10 min | ASTM D1238 | 4 | <0.15 | H | | 3 | <0.4–0.15 | P | 3 | <0.4–0.15 | P | |
| Flex, mod., MPa | ASTM D790 | 5 | 760–<1,100 | P | | 5 | 760–<1,100 | P | 4 | 550–760 | P | |
| Tensile yield strength, MPa | ASTM D638, Type IV | 4 | 20.7–24 | P | | 4 | 20.7–24 | P | 4 | 20.7–24 | P | |
| ESCR[a], hour at F20 | ASTM D1693 | 3 | 192 | F | | 3 | 192 | P | 3 | 192 | na | na |
| Carbon black, % | ASTM D4218 | C | >2 | L | L | C | >2 | P | C | >2 | Some low | |
| SCGR[b], hour | ASTM F1473 | 0 | NS | — | — | 0 | NS | — | 0 | NS | — | |
| HDB[c], MPa | ASTM D2837 | 3 | 8.6 | — | — | 3 | 8.6 | — | 0 | NS | — | |
| SP-NCTL, hour at 15% σy | — | — | — | 3–4 | 2–34 | — | — | 80 | — | — | — | |
| SP-NCTL, hour at 25% σy | — | — | — | — | — | — | — | 19 | — | — | 243 | 16 |
| OIT, minute | — | — | — | 1.3 | 2–8 | — | — | 14.2 | — | — | 15–18 | 15–18 |

[a]ESCR=environmental stress crack resistance.

[b]SCGR=slow crack growth resistance.

[c]HDB=hydrostatic design basis.

[d]P=pass; F=fail; H=high; L=low; NS=not specified; and na=not available.

[e]SP-NCTL=single point notched constant tensile load.

[f]OIT=oxidative induction time.



J. Mater. Civ. Eng., 2006, 18(4): 581-587

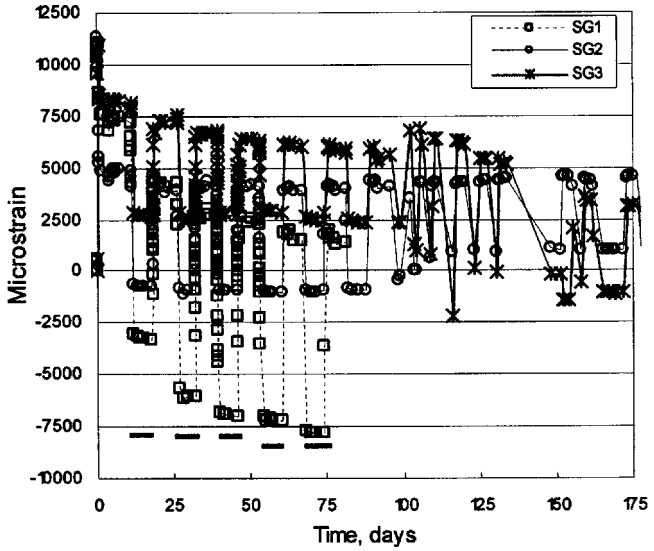


**Fig. 4.** Strain versus time history as determined by gauges on Specimen B2 (bars near the bottom-left indicate periods at ambient temperature); gauge SG1 failed after about 80 days

similar fatigue behavior and had the lowest fatigue resistance. The two new PE3408 duct specimens behaved similarly and exhibited the highest resistance. Results for specimens from the SM and LK bridges were intermediate. As such, the order of the fatigue resistance of these six ducts conforms to that of the stress crack resistance (SCR) measured by the SP-NCTL test (see Table 3).

### *Simulated Tendon Experiments*

Fig. 4 shows a plot of microstrain versus time for Specimen B2 for the three gauge locations (SG1, SG2, and SG3) indicated in Fig. 2. The initially high positive (tensile) strain for all gauges reflects the initial pressurization. Output from all three gauges dropped about 20–25% upon pressure release, followed by a further strain decrease with time. The cyclic variation coincided with the thermal cycling and was generally reproducible from one cycle to the next, although an overall downward trend is apparent. The magnitude of these strain changes was greatest for SG1, followed by SG2 and SG3. Note, however, that microstrain was lowest when the specimen was exposed to a high (ambient) temperature and vice versa. This seems counterintuitive as decreasing

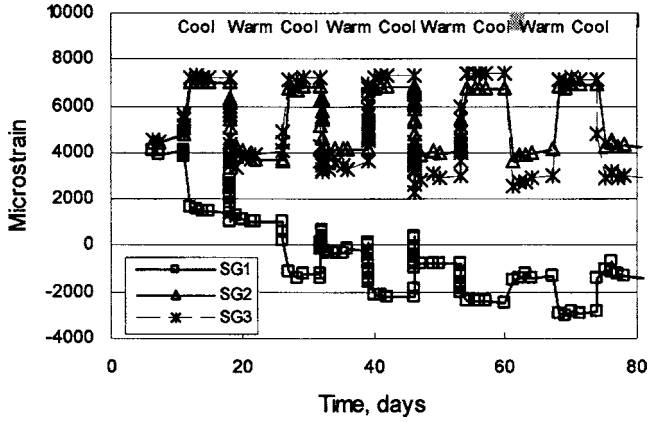


**Fig. 5.** Corrected strain versus time for Specimen B2

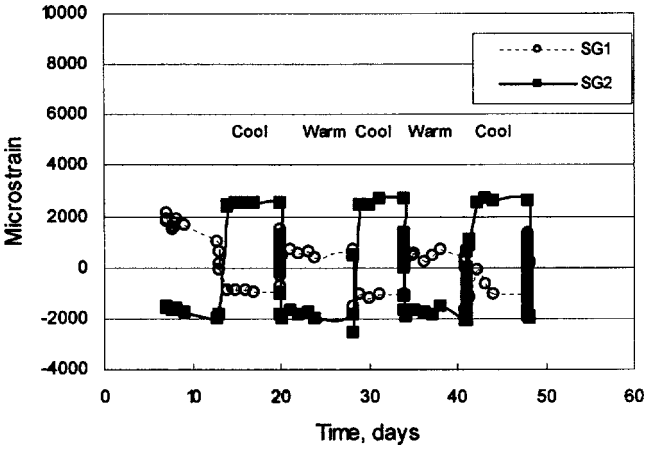


**Fig. 6.** Corrected strain versus time for Specimen B4

temperature should cause the duct, which has a higher coefficient of thermal expansion than the grout, to contract around the grout and yield a progressively greater tensile stress state with decreasing temperature. To address this, the strain gauge data were re-evaluated by, first, calculating the thermal expansion coefficient of several PE3408 duct samples (average value 117 microunits $\cdot\,^{\circ}C^{-1}$) and, second, subtracting the duct dimensional change that resulted from this cause from the measured strain.

Fig. 5 is a corrected strain versus exposure time plot for Specimen B2 for the time span during which SG1 functioned. This indicates that the corrected outputs for SG2 and SG3 were similar, with the cyclic strain being highest at low temperature and the lowest at high. This trend is reversed, however, for SG1 and, in addition, is displaced to lower strain. Fig. 6 shows a comparable plot for Specimen B4 (no SG3 gauge was employed for this specimen).

The cyclic strain output between gauges SG2 and SG3 compared to SG1 differed because contraction of the duct around the grout introduced a tensile hoop stress only at the location of SG3 but bending strains occurred at the other two locations as a result of the presence of the air void channel. This is illustrated schematically by Fig. 7.

Subsequent to the experiments, the specimens were dissected and the size of the grout void channel along the top of the tendon interior was measured. Fig. 8 shows the grout and void channel at the mid-specimen length (the location of gauges SG1 and SG2) of

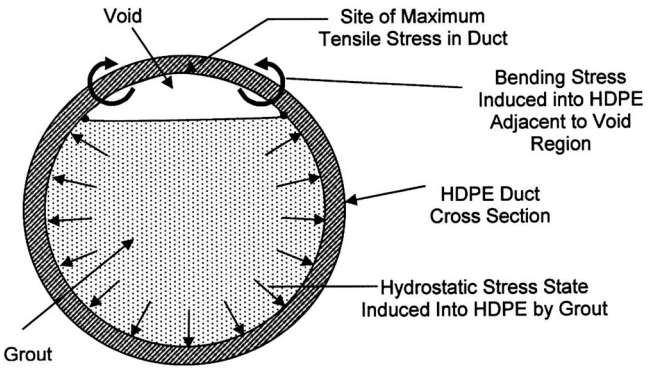


**Fig. 7.** Bending stresses in duct above grout void



J. Mater. Civ. Eng., 2006, 18(4): 581-587

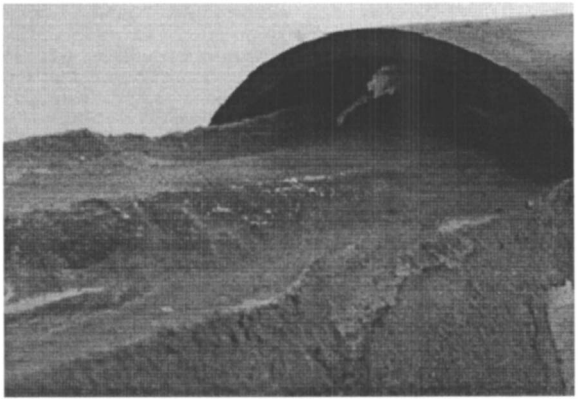

**Fig. 8.** Void channel in Specimen B4 at location of strain gauges SG1 and SG2 in perspective to section of duct

Specimen B4. The higher strain range indicated by SG2 for Specimen B2 compared to B4 probably resulted from the larger SDR and smaller grout void for Specimen B2.

### *Finite-Element Analysis (FEA)*

A finite-element analysis was performed using a two-dimensional ANSYS model of a tendon cross-section with an SDR 21 duct and a grout void that comprised either 3, 8, or 10% of the interior. Triangular, six-node elements were employed. A general illustration of the mesh is show in Fig. 9. An expanded view of the modeled duct section above the grout void is shown in Fig. 10. Stress-strain response of both duct and grout was considered to be linearly elastic with modulus $1.01\times10^3$ MPa (146 ksi) for the former (CSR Company, "HDPE EHMW PE3408 pipe." *2706 N.I-35 (76240)*, Gainesville, Tex.) and $2.80\times10^3$ MPa (406 ksi) for the latter (Chandrupatla and Belegundu 2002).

The simulation assumed pressurization of the tendon until the grout set, and depressurization was modeled as a corresponding 30°C temperature drop. This temperature change was determined to be equivalent to a 0.414 MPa (60 psi) internal pressure decrease. Additionally, a 41.6°C temperature drop, which corresponds to a 0.518 MPa (75 psi) pressure decrease, was also modeled. The duct coefficient of thermal expansion was the same as indicated above (117 microunits°$C^{-1}$) and for the grout $10\times10^{-6}$ microunits° $C^{-1}$, as measured from an SSK sample using the same procedure. Poisson's ratio for the duct and grout were taken as 0.28 and 0.21, respectively (CSR Company).

**Fig. 9.** FEA mesh

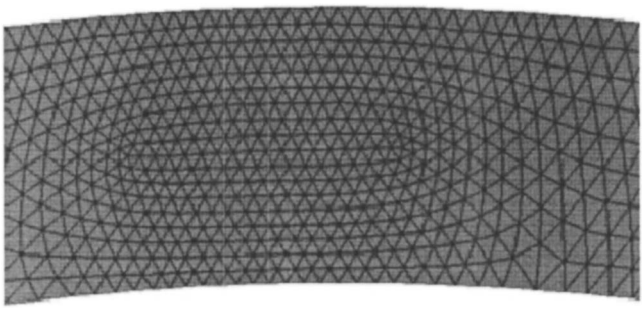

**Fig. 10.** Expanded view of FEA mesh in region above air void

An example of the FEA results is shown in Fig. 11 as a color contoured plot of the first principal (hoop) stress for the case of 0.414 MPa (60 psi) grouting pressure and 3% void volume. This projects that tensile stress was highest at the location of SG2 and at the outer duct surface opposite the grout void corner (one on each side). Table 4 lists the FEA computed stress at each of these three locations for the above two grouting pressures and three void volumes. Corresponding, Fig. 12 summarizes the stress range at each of these three locations (stress range is taken as from zero, which should occur at the grouting temperature, to the respective value determined from FEA) as a function of void size and grouting pressure. For the smallest model void size (3%), stress was greatest at the corner locations and next greatest at the SG2 site. These stresses decrease with increasing void size and merge with measured values from the simulated tendon specimens (Figs. 5 and 6) for which void volumes at the strain gauge locations were measured as 16 and 10% for Specimens B2 and B4, respectively. This apparent agreement may seem fortuitous because the experimental simulated tendon data were for a 60°C temperature range, whereas the FEA model is based on a 30°C range; however, the grout heat of hydration should reduce this difference. In all cases, stress was greater for the higher grouting pressure. Also shown is the stress range projected for SG3 of Specimen B2, which is about 50% of the maximum bending, void apex stress (3% void area). Stress at the SG3 location should be independent of void size. The same duct elastic modulus as for the FEM models ($1.01\times10^3$ MPa) was assumed in converting from strain to stress.

### *Analysis of Fatigue Data Using FEA*

The fatigue data in Fig. 3 were evaluated using results of the FEA. In doing this, consideration was given to residual stresses that the actual ducts likely contained, but that the fatigue test specimens, which were prepared from molded plaque, did not. Residual stress determinations could not be made for field acquired samples because it was not possible to obtain complete, intact circumferential sections. However, residual stresses were measured on samples of PE3408-1 with three different SDR and on duct from Specimen B2 (SDR 21) subsequent to the simulated tendon experiments by two techniques: Method 1, based on strain change indicated by transversely oriented gauges, and Method 2,



J. Mater. Civ. Eng., 2006, 18(4): 581-587

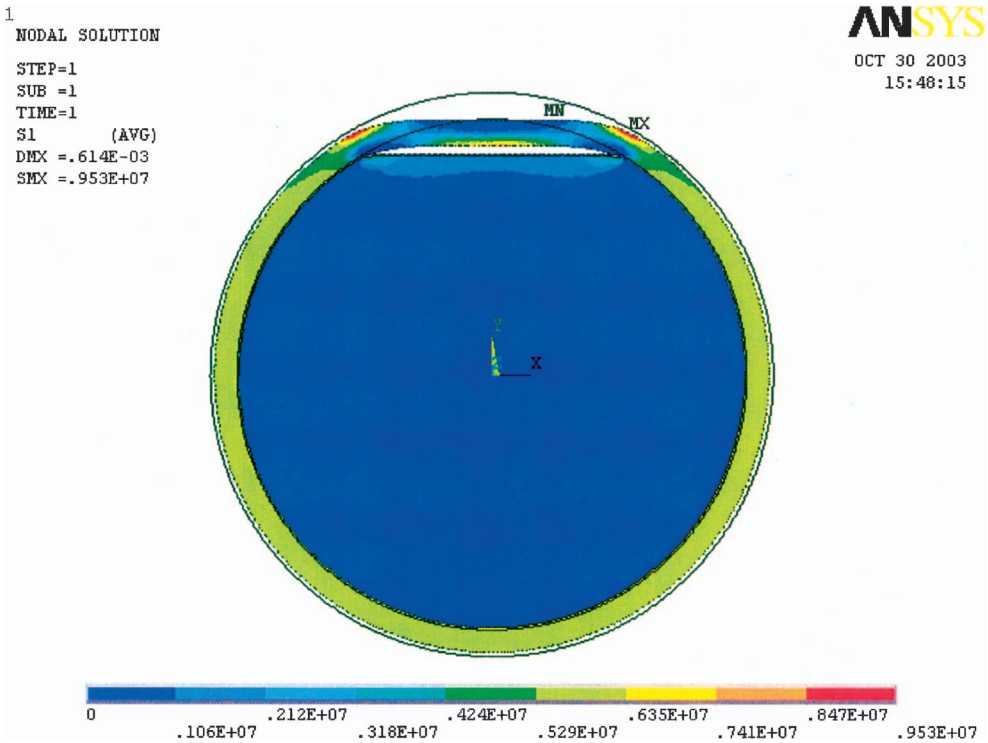


**Fig. 11.** (Color) FEA result showing principal stress (hoop) in cylindrical coordinates for duct with 3% grout void and grouting pressure 0.414 MPa (0.60 ksi) (color-coded units on graph in Pa)

which involved measurement of duct diameter change subsequent to removing a longitudinal duct section. The results are shown in Table 5 and indicate that the average residual stress measured by Method 2 was 6.6 MPa, which is about 60% higher than that measured by Method 1. Considering such a residual stress, the highest absolute stress (thermal contraction induced plus residual) was at the interior void apex position (SG2 location in the simulated tendon tests, see Fig. 2) because the residual stress on the exterior duct surface was compressive. This is consistent with the finding that cracks in the MB ducts were typically close to the 12 o'clock orientation and were initiated from the interior surface (Hartt and Venugopalan 2002). If then the thermal contraction induced stress on the duct interior is taken as 10.0 MPa (Fig. 11) and a residual stress of 6.6 MPa is added to this, a new absolute tensile stress of (16.6 MPa) results. Both the FEA and simulated tendon experiments indicate that cyclic stressing as a consequence of temperature changes can also occur in the absence of grout voids (Fig. 11); however, the stress range is of lower magnitude in this case.

**Table 4.** Localized Duct Stress as a Function of Grouting Pressure and Void Volume

| Pressure, MPa (psi) | Void volume, percent | Stress, MPa (ksi) | | |
|---|---|---|---|---|
| | | SG2 | SG3 | Corner |
| 0.414 (60) | 10 | 5.38 (0.78) | 6.72 (0.97) | 6.72 (0.97) |
| 0.518 (75) | | 6.06 (0.88) | 7.57 (1.10) | 7.57 (1.10) |
| 0.414 (60) | 8 | 6.47 (0.94) | 6.47 (0.94) | 8.32 (1.21) |
| 0.518 (75) | | 7.29 (1.06) | 6.25 (0.91) | 9.38 (1.36) |
| 0.414 (60) | 3 | 8.47 (1.23) | 6.35 (0.92) | 9.53 (1.38) |
| 0.518 (75) | | 9.55 (1.38) | 7.16 (1.04) | 10.7 (1.55) |

The data in Fig. 3 indicate that a stress range of 16.6 MPa corresponds to failure of the MB and SSK specimens at less than $10^3$ cycles. Considering that the in-service ducts experienced one thermally induced stress cycle per day, cracking will likely occur in ducts in these two bridges several years after construction. For the Seven Mile and Long Key Bridges, the cycles to failure corresponding to the above fatigue strength (16.6 MPa) is approximately $2 \cdot 10^4$ or 50-plus years. For ducts utilizing the PE3408 resins, this time is more than 100 years. This, of course, assumes that no significant long-term detrimental reactions, such as antioxidant depletion, compromise the mechanical properties of the bridges.

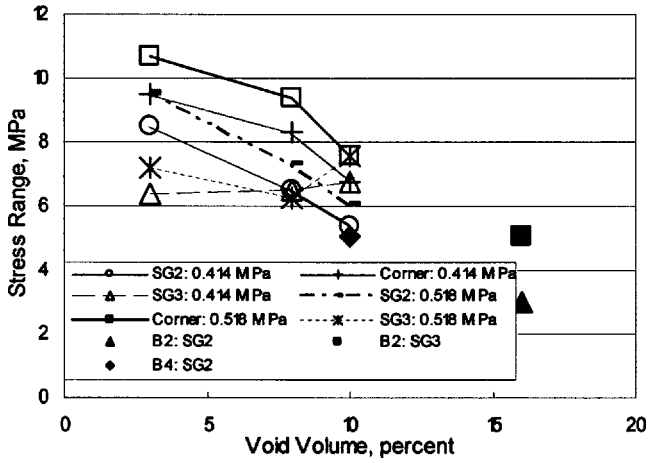


**Fig. 12.** Local duct stress as function of position, level of pressurization during grouting setting, and void volume



J. Mater. Civ. Eng., 2006, 18(4): 581-587

**Table 5.** Results of Residual Stress Determinations

| Material specimen number | Strain change, microunits (Method 1) | Stress, MPa (Method 1) | Stress, MPa (Method 2) |
|---|---|---|---|
| SDR 17 | 5249 | 4.92 | 6.89 |
| SDR 21 | 3540 | 3.32 | 5.42 |
| SDR 26 | 3530 | 3.31 | 5.89 |
| Specimen B2 | 5510 | 5.19 | 8.23 |

### *Duct Specification*

As a consequence of this research and related FDOT studies, smooth duct for posttensioning tendon bridge systems must now meet the following requirements:

1. Fabrication must use 100% virgin polyethylene resin that meets the requirements of ASTM D3350 with a minimum cell class of 344464C.
2. Resin must contain antioxidant(s) such that the minimum oxidative induction time (OIT) is 40 min, according to ASTM D3895.
3. The dimension ratio (diameter to thickness) must be 17.0, as established by either ASTM D3055 or ASTM F714.
4. The minimum pressure rating (working pressure) must be 100 psi (0.69 MPa).

## Conclusions

1. Fatigue tests were performed on plaques prepared from HDPE duct samples acquired from four segmentally constructed Florida bridges: Mid-Bay (MB), Sunshine Skyway (SSK), Seven Mile (SM), and Long Key (LK). They were also performed on specimens prepared from two new ducts based on PE3408 resin. Cycles to failure at any given stress range was lowest for the SSK and MB specimens, intermediate for the SM and LK, and highest for ones prepared using the two new PE3408 resins. These results are consistent with those from material property determinations that indicated this same ranking based upon stress cracking resistance.
2. Results from experiments in which strain-gauge-instrumented simulated tendon specimens were exposed to cyclic temperature variations indicated that fatigue stressing can arise from thermal changes. Finite element analysis of a modeled tendon indicated that stress range is greatest on the internal duct surface at the apex of longitudinal grout air voids and is inversely proportional to SDR and to air void volume.
3. The finite element analysis and the fatigue data suggests that ducts on the MB and SSK bridges probably began cracking after several years in service, whereas those on the SM and LK bridges should have 50-plus years of crack-free service, assuming that material properties do not degrade with time.

## Acknowledgments

The authors are indebted to the Florida Department of Transportation (FDOT) for financial support of this research and for helpful guidance and access to structures throughout. Appreciation is expressed to Mr. George Jones, Mr. Florent David, and Miss Cynthia Baxindine for assistance with the experiments. The opinions expressed are those of the authors and not necessarily the FDOT.

## References

Chandrupatla, T., and Belegundu, A. (2002). *Introduction to finite elements in engineering*, 3rd Ed., Prentice-Hall, N.J.

Corven Engineering. (2001). "Mid-Bay Bridge posttensioning evaluation." *Final Rep. Submitted to Florida Department of Transportation District 3*.

Corven Engineering. (2002). "New directions for Florida posttensioned bridges." *Final Rep. Submitted to Florida Department of Transportation*.

Ghorbanpoor, A., and Madathanapalli, S. C. (1993). "Performance of grouts for posttensioned bridge structures." *Rep. No. FHwA-RD-92-095*, Federal Highway Administration, Washington, D.C.

Hartt, W. H., Hsuan, G., Suarez, J., Zhang, J., and David, F. (2005). "The role of polyethylene duct cracking in failure of posttensioning cables in Florida segmental bridges." *Final Rep. Submitted to Florida Department of Transportation on Project BD220*.

Hartt, W. H., and Venugopalan, S. (2002). "Corrosion evaluation of posttensioned tendons on the Mid-Bay Bridge in Destin, Florida." *Final Rep. Submitted to Florida Department of Transportation by Florida Atlantic Univ*.

Pressure Pipe Institute. (2005). "PPI listing of hydrostatic design basis (HDB), strength design basis (SDB), pressure design basis (PDB), and minimum required strength (MRS) ratings for thermoplastic piping materials or pipe." *Publication TR-4/2005*, Washington, D.C.

Tabatabai, H., Ciolko, A. T., and Dickson, T. J. (2000). "Implications of test results from full-scale fatigue tests of stay cables composed of seven-wire prestressing strand." *Proc., 4th Int. Bridge Engineering Conf.*, Vol. 1, Transportation Research Board, National Research Council, Washington, D.C.



J. Mater. Civ. Eng., 2006, 18(4): 581-587